Motor and Tail Homology 1 (TH1) Domains Antagonistically Control Myosin-1 Dynamics

Jessica N. Mazerik,[†] Lewis J. Kraft,[‡] Anne K. Kenworthy,[‡] and Matthew J. Tyska[†*]
[†]Department of Cell and Developmental Biology and [‡]Department of Molecular Physiology and Biophysics, Vanderbilt University Medical Center, Nashville, Tennessee

ABSTRACT Class 1 myosins are monomeric motor proteins that fulfill diverse functions at the membrane/cytoskeletal interface. All myosins-1 contain a motor domain, which binds actin, hydrolyzes ATP, and generates forces, and a TH1 domain, which interacts directly with membrane lipids. In most cases, TH1 is needed for proper subcellular localization and presumably function, although little is known about how this domain regulates the behavior of class 1 myosins in live cells. To address this, we used single molecule total internal reflection fluorescence microscopy to examine the dynamics of the well-characterized myosin-1a isoform during interactions with the cortex of living cells. Our studies revealed that full-length myosin-1a exhibits restricted mobility relative to TH1 alone. Motor domain mutations that disrupt actin binding increased the mobility of full-length myosin-1a, whereas mutations to the TH1 domain that are known to reduce steady-state targeting to the plasma membrane unexpectedly reduced mobility. Deletion of the calmodulin-binding lever arm in Myo1a mimicked the impact of actin-binding mutations. Finally, myosin-1b, which demonstrates exquisite sensitivity to mechanical load, exhibited dynamic behavior nearly identical to myosin-1a. These studies are the first, to our knowledge, to explore class 1 myosin dynamics at the single-molecule level in living cells; our results suggest a model where the motor domain restricts dynamics via a mechanism that requires the lever arm, whereas the TH1 domain allows persistent diffusion in close proximity to the plasma membrane.

INTRODUCTION

Class 1 myosins are widely expressed, monomeric motor proteins that function at the actin/membrane interface in membrane tension maintenance (1), mechanotransduction (2), and membrane trafficking and remodeling (3,4). The eight vertebrate class 1 myosins (Myo1a–h) exhibit diverse expression and localization but share defining structural features including an actin-binding, ATP-hydrolyzing motor domain that generates mechanical force, a force transducing neck region (also known as a lever arm) that binds varying numbers of calmodulin light chains, and a TH1 domain that interacts directly with cellular membranes. Although the biochemical and biophysical properties of these domains are well studied (5,6), investigators are just beginning to ask how the activities of these domains are integrated to control the function of these motors in living cells.

For proteins to perform specific biological functions, they must first target to the proper subcellular compartment. In the context of class 1 myosins, which are structurally and kinetically incapable of long-range directed movement along the actin cytoskeleton (5,7), these molecules likely exploit diffusion to search for sites of cellular function. The molecular motion observed during this diffusive search we refer to herein as dynamics. The overarching goal of this study was to investigate mechanisms that control class 1 myosin dynamics in cells.

Class 1 myosins in general are slow, low duty ratio motors that spend a small fraction of their total ATPase cycle strongly bound to actin (5,7). Recent in vitro optical trapping studies, however, have determined that some isoforms respond to mechanical load by increasing their actin-attached lifetime and thus, duty ratio (8,9). For myosin-1b (Myo1b), small (<1 pN) opposing forces increase the lifetime of the strongly bound state dramatically (8) suggesting function as an anchor in the presence of load. In the case of myosin-1c, actin-attached kinetics are only impacted by larger forces, suggesting function as a slow power generator (9). Myosin-1a (Myo1a) also exhibits properties that predict a capacity for tension sensing (10–12), although a direct test of this prediction using optical trapping approaches has yet to be performed. How motor domain activity and specifically load sensing impact the dynamics of class 1 myosins in living cells has not been investigated.

Myosin-1 TH1 domains exhibit long-lived interactions with membranes (13–15) and are required for steady-state targeting in cells (15–18), even in the few cases where the motor domain enhances localization (17,18). Several motifs within TH1 have been implicated in membrane binding. A Myo1 pleckstrin homology motif, first discovered within the Myo1c TH1 domain, mediates tight and stereo-specific binding to $PI(4,5)P_2$ in vitro and in cells (19,20). Mutating basic residues in this region disrupts the subcellular targeting of Myo1b, -1c, -1g, and -1f (18–21). Although this domain is conserved, studies with Myo1a, Myo1e, and *Acanthamoeba* myosin-1c suggest that different isoforms might employ distinct or additional mechanisms for

Submitted October 15, 2013, and accepted for publication December 26, 2013.

*Correspondence: matthew.tyska@vanderbilt.edu

Editor: E. Ostap.

0006-3495/14/02/0649/10 $2.00

http://dx.doi.org/10.1016/j.bpj.2013.12.038

targeting to sites of function in cells (22–24). For example, in the context of Myo1a, perturbation of the pleckstrin homology domain has a minimal impact on subcellular targeting (22). Instead, two distinct membrane-binding motifs within TH1 referred to as the N-terminal (NTM) and C-terminal (CTM) targeting motifs, promote localization (22). Our previous studies suggest that these motifs bind membrane through electrostatic interactions. Myo1a binds phosphatidylserine-containing liposomes in vitro, and alanine substitution of basic residues in either of these TH1 regions decreases membrane-bound lifetime and disrupts steady-state targeting in cells (22). Mutations in Myo1a CTM have also been linked to a loss of epithelial polarity and development of colorectal cancer (25). Together, these studies highlight the importance of TH1/membrane interactions and suggest a model where TH1 serves as a master regulator of myosin-1 dynamics.

Using the well-characterized Myo1a isoform as a model class 1 myosin, we sought to test the hypothesis that the TH1 domain controls myosin-1 dynamics in cells. To this end, we employed single molecule total internal reflection fluorescence (SM-TIRF) microscopy in combination with single particle tracking and mean-squared displacement (MSD) analysis to examine the dynamics of Myo1a interacting with the cortex of living cells. Our results show that the Myo1a motor and TH1 domains act antagonistically to control the dynamics of this molecule; motor domain interactions with actin restrict mobility, whereas TH1 interactions with membrane promote two-dimensional diffusion close to the cell surface. Deletion of the neck region significantly increases the mobility of Myo1a. We also find that full-length Myo1a dynamics are strikingly similar to those observed for the load-sensing motor, Myo1b. To our knowledge, this study is the first to explore myosin-1 dynamics with single-molecule resolution in cells and as such, provides novel insight as to how myosin-1 mobility is controlled in the complex cellular environment.

MATERIALS AND METHODS

SM-TIRF microscopy

Myo1a constructs were tagged with 3x-mCitrine (26) and expressed in LLC-PK1-CL4 cells. Single-molecule imaging was performed on live cells using a slight modification of our previously published procedure (22). For these experiments, a Photometrics Evolve EM-CCD camera (Photometrics, Tucson, AZ) was used to collect image stacks, and image acquisition was controlled with Nikon Elements software (Nikon, Melville, NY). Calibrated pixel size was 110 nm/pixel. 488-nm and 561-nm LASERs were used to excite constructs of interest tagged with 3x-mCitrine or mCherry-Espin (a label for F-actin), respectively. Acquisition parameters were adjusted to optimize temporal resolution, which enabled us to acquire time-lapse data of single-molecule dynamics at higher frame rates; data were collected using a 2-frame rolling average at 50 fps for 400 frames. To increase the signal/noise ratio of single molecules spots at higher frame rates, we increased excitation LASER power, which also had the effect of reducing spot lifetimes relative to our previous observations (22).

MSD analysis

For single particle tracking, ImageJ was used to enhance contrast and threshold image stacks to highlight only the brightest particles on the ventral surface, which typically exhibited an 8-bit grayscale value of 120–130. Particles were then tracked using DiaTrack (Semasopht, North Epping Australia) (27). For each construct, trajectories were sampled from 20 to 40 cells. Trajectories produced in DiaTrack were subjected to further analyses using software written in MATLAB (The MathWorks, Natick, MA). MSD for each trajectory with lifetime greater than or equal to 10 frames was calculated using all pairs of points with the appropriate lag times (28). For N time points, the nth average is as follows, where r is particle displacement:

$$\left\langle r^2(n)\right\rangle = \frac{1}{N}\sum_{i=0}^{N-1}[r(i+n)-r(i)]^2 \quad (1)$$

The MSD was cut off at one-half of the total number of time steps before fitting to a two-dimensional simple diffusion model:

$$\left\langle r^2(t)\right\rangle = 4Dt \quad (2)$$

D values were obtained for each trajectory that lasted at least 10 frames (200 ms) and for each subsequent 10-frame interval, which resulted in multiple D values for individual trajectories lasting $\geq$20 frames (28). To allow for quantitative comparisons to be made between constructs, diffusion coefficients calculated from single-molecule events were plotted in histograms using SigmaPlot v.10, normalized for amplitude, and fit to log-Gaussian distributions using Prism v.6 (28,29) to obtain values for peak D. We also calculated a shape factor for the resulting distributions as σ/Peak D where σ and Peak D are free parameters (width and mean, respectively) from log-Gaussian fits. Here, lower values represented broader distributions that were generally shifted toward higher D values. Kymograph analysis was performed on image stacks using ImageJ. Maximum intensity projections of 3x-mCitrine constructs (*green*) and mCherry-Espin (*red*) image stacks were contrast enhanced, merged, and pseudocolored using ImageJ.

RESULTS

Myo1a exhibits restricted mobility relative to TH1 alone

Myo1a is one of the most well-characterized vertebrate class 1 myosins; it is highly expressed in the small intestine where it localizes to brush border microvilli on the apical surface of enterocytes (30). In the brush border, Myo1a links the core actin bundles of microvilli to the overlying plasma membrane and plays key roles in maintaining overall structure (31), regulating membrane tension (1), and facilitating microvillar vesicle shedding (32). Previously, we measured lifetimes for the TH1/membrane interaction at the ventral surfaces of LLC-PK1-CL4 epithelial cells using SM-TIRF (22). These experiments provided insight as to how the NTM and CTM govern TH1 membrane-bound lifetime. They did not, however, explore the diffusion of TH1 or full-length Myo1a, or examine how specific structural features regulate these dynamics.

In this study, our goal was to understand how the dynamics of Myo1a are controlled at the actin-rich cell periphery. We used SM-TIRF microscopy to image tagged

Myo1a constructs expressed in live epithelial cells in a manner similar to our previous report (22). We transiently expressed 3x-mCitrine-tagged Myo1a constructs in LLC-PK1-CL4 cells stably expressing mCherry-Espin to colabel F-actin. Because this cell line does not express endogenous Myo1a or any of its putative binding partners (15,33,34), our expectation was that observed dynamics should only reflect interactions with membrane and actin. Single-molecule events at the ventral surface were recorded over time and the resulting image stacks were subject to single particle tracking and MSD analysis to extract diffusion coefficients (D) as a readout for molecular mobility.

We first examined the mobility of full-length Myo1a and TH1 (Fig. 1). As a point of comparison, we also imaged the dynamics of Lactadherin-C2 (Lact-C2) (35). Lact-C2 competes with Myo1a-TH1 for binding sites in microvilli, and both proteins bind to phosphatidylserine (22,35). The D distribution for full-length Myo1a was characterized by a peak D of 0.031 $\mu m^2/s$ with a relatively narrow shape factor of 33.9 (Fig. 2 *A*, Table 1). Myo1a also exhibited a significant population of events that were nearly immobilized (Fig. 2 *A*, *red arrowhead*). In contrast, TH1 and Lact-C2 D distributions were much broader and right-shifted (i.e., toward higher mobility) relative to the full-length Myo1a data set (Fig. 2, *B* and *C*). These distributions exhibited higher peak D values of 0.089 $\mu m^2/s$ and 0.116 $\mu m^2/s$, and lower shape factors of 10.2 and 6.3 for TH1 and Lact-C2, respectively (Table 1). The D values measured here are significantly lower than those measured for lipid-modified proteins (D = 0.25–1 $\mu m^2/s$) (36,37), but are in a range consistent with the diffusion of transmembrane or peripherally associated membrane proteins (D = 0.004–0.1 $\mu m^2/s$) (38–40). Differences between the full-length Myo1a and TH1/Lact-C2 D distributions were also qualitatively visible in raw trajectory data (Fig. 2 *D*). Additionally, TH1 and C2 lacked the long-lived, low mobility events that were present in the full-length Myo1a data set (Fig. 2 *A*, *inset*, *arrowheads*). The differences observed between full-length Myo1a and TH1 dynamics could, in part, be related to their different molecular masses (~206 kDa for full-length Myo1a versus ~126 kDa for TH1). However, peak D values for both constructs are two orders of magnitude lower than expected for freely diffusing proteins in solution (41). Thus, D values measured in this assay are likely dominated by interactions with specific subcellular compartments, such as the actin cytoskeleton and/or plasma membrane.

These initial results suggest a fundamental difference between the diffusive properties of TH1 and Lact-C2, which interact primarily with membrane, and full-length Myo1a, which can interact with both membrane and actin filaments. Indeed, kymographs of Myo1a recordings revealed striking examples of nearly immobilized molecules that colocalized with F-actin for many seconds (Fig. 3 *A*, *white dashed lines adjacent to events*). In contrast, TH1 molecules showed significant lateral movement and rarely colocalized with actin filaments (Fig. 3 *B*). Together, these results suggest that the motor domain and/or neck regions might function to restrict the mobility of full-length Myo1a at the actin-rich cell cortex.

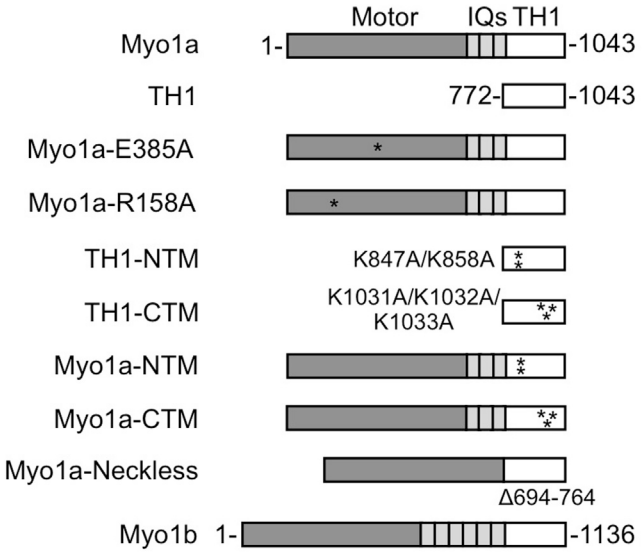

FIGURE 1 Constructs used in this study. Point mutations E385A and R158A in the motor domain are predicted to result in weak actin binding. Point mutations K847A/K858A and K1031A/K1032A/K1033A in NTM and CTM are predicted to disrupt membrane binding. Myo1a-Neckless has functional motor and tail domains, but lacks the lever arm.

The motor domain limits the mobility of full-length Myo1a

To determine if motor domain actin-binding activity restricts Myo1a dynamics in cells, we made single amino acid mutations to disrupt mechanochemical function. We targeted R158 and E385, which are absolutely conserved residues found in the active site of all myosin superfamily members (42)(Fig. 1). We strategically chose to mutate this pair of residues because crystal structures of the *Dictyostelium* myosin-2 motor domain revealed that the equivalent residues (R238 and E459) form a salt bridge at the interface of switch I and switch II in the core of the active site (43). Mutations at these positions phenocopy each other with regard to impact on ATP hydrolysis and actin binding, and trap the motor in a weak actin-binding state (44,45). Alanine substitutions at both of these positions give rise to significant loss of basal and actin-activated ATPase activity, failure of ATP hydrolysis in single turnover experiments, inability to move F-actin in sliding filament assays, and failure to form rigor complexes with F-actin. In the context of sliding filament assays, actin filaments do not remain bound to R158 mutant myosin-coated surfaces, again suggesting that these motors are unable to enter

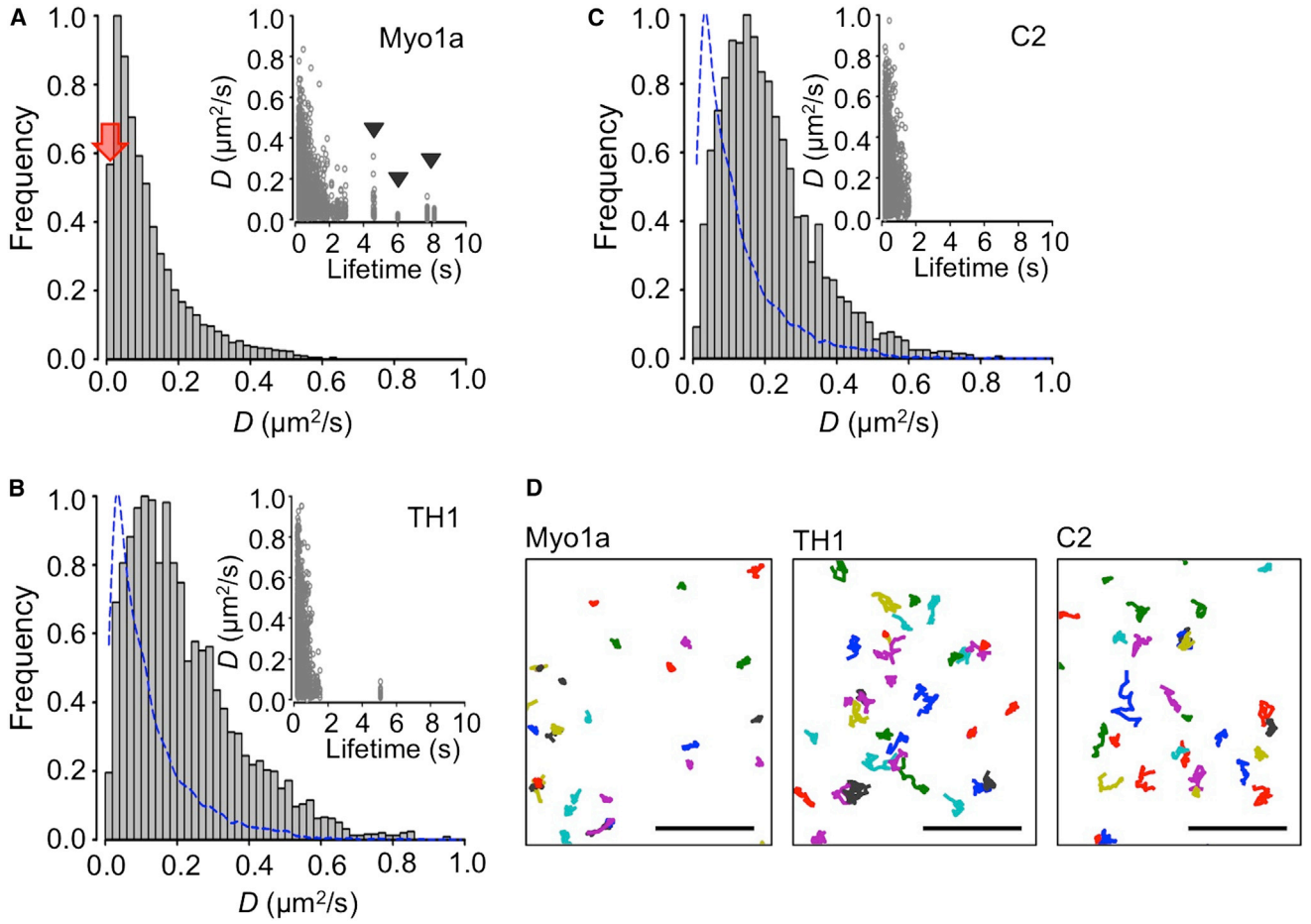

FIGURE 2 Single-molecule dynamics of Myo1a, Myo1a-TH1, and Lact-C2. Histograms of *D* values were normalized then plotted for Myo1a (*A*), Myo1a-TH1 (*B*), or Lact-C2 (*C*). Inset, plots of *D* versus lifetime associated with each trajectory. Myo1a displayed slower overall dynamics as compared to Myo1a-TH1 and Lact-C2. Numerous long-lived events with low mobility were detected for Myo1a (*black arrowheads*, *inset*) and were rarely detectable for Myo1a-TH1 and Lact-C2. Myo1a also displayed a shift toward slower mobility and had many more low mobility events (*red arrowhead*). Blue dashed lines are traced outlines of Myo1a histogram density. (*D*) Representative *x*, *y* plots of randomly selected trajectories for Myo1a, TH1, or Lact-C2. Events have a minimum lifetime of 30-frames (600 ms). Trajectories are randomly colored to facilitate visualization. Scale bars are 4 μm.

a strongly bound state. Interestingly, mutations at the conserved R158 position in myosin-7a are linked to Usher syndrome, an inherited sensory disorder (46). Finally, others have successfully used a similar approach to study the functional significance of motor activity in the context of myosins-6 and -15 (47,48).

If the lower mobility of full-length Myo1a relative to TH1 is due to actin binding, alanine substitutions at R158 and E385 should cause the *D* distribution to shift toward higher values. Indeed, *D* distributions observed for both Myo1a-E385A and Myo1a-R158A were both right-shifted with peaks broader than that of Myo1a, centered at 0.059 μm^2/s and 0.050 μm^2/s, respectively (Fig. 3, *C* and *D*, Table 1). The broadening of these distributions was also reflected in reduced shape factors relative to full-length Myo1a (Table 1). The fraction of events showing near immobilization (Fig. 1 *A*, *red arrowhead*) was also reduced (Fig. 3). Interestingly, the long-lived events that were present in Myo1a records (Fig. 2 *A*, *inset*) were absent from Myo1a-R158A and Myo1a-E385A (Fig. 3, *inset*). Together, the data suggest that the restricted mobility observed for full-length Myo1a is at least partially due to interactions between the motor domain and actin filaments at the cell surface.

TH1/membrane interactions also influence Myo1a dynamics

We next sought to determine the extent to which TH1/membrane interactions influence the dynamics of full-length Myo1a in cells. Our previous studies showed that two membrane binding motifs, NTM and CTM, are required for steady-state targeting of TH1 and Myo1a, and disruption of either of these regions results in decreased membrane-bound lifetimes in cells (22). We investigated the effects of mutations to these motifs (NTM, K847A/K858A and CTM, K1031A/K1032A/K1033A) on the mobility of TH1 and full-length Myo1a. Strikingly, membrane-binding mutations to either the NTM or CTM markedly reduced

TABLE 1 Summary of *D* distribution parameters

Construct[a]	n[b]	Peak D ($\mu m^2/s$)[c]	Shape factor[d]
Myo1a	4234	0.031 ± 0.0003	33.9
TH1	3842	0.089 ± 0.003	10.2
Lact-C2	3733	0.116 ± 0.003	6.3
Myo1a-R158A	3955	0.050 ± 0.001	17.1
Myo1a-E385A	5702	0.059 ± 0.001	15.2
TH1-NTM	977	0.028 ± 0.0004	35.1
TH1-CTM	1067	0.026 ± 0.001	39.0
Myo1a-NTM	970	0.027 ± 0.0002	31.7
Myo1a-CTM	2751	0.027 ± 0.0004	33.5
Myo1a-Neckless	3381	0.061 ± 0.002	14.4
Myo1b	5633	0.033 ± 0.0004	29.0

[a]All constructs were tagged with N-terminal 3xmCitrine.
[b]n, number of single-molecule events that were compiled into D distributions.
[c]Fit parameter ± SE of the fit; all fits are shown in Fig. S1.
[d]Calculated as σ/Peak D where σ and Peak D are free parameters from log-Gaussian fits.

mobility in both cases (Fig. 4, Table 1). In the case of TH1, peak D was reduced to 0.028 $\mu m^2/s$ by NTM mutations and 0.026 $\mu m^2/s$ by CTM mutations. Full-length Myo1a diffusion coefficients were slightly reduced to 0.027 $\mu m^2/s$ in both cases (Table 1). These results were intriguing because our previous studies show that in the context of TH1, these mutations reduce membrane-bound lifetime and steady-state targeting (22). Therefore, membrane-bound lifetime can be uncoupled from diffusive mobility, i.e., low mobility events do not have to be long-lived. The shift toward lower mobility for NTM and CTM mutants indicates that the multiple basic motifs in the TH1 domain allow Myo1a to diffuse near the membrane in a high mobility state.

A functional lever arm is required for the restricted mobility of full-length Myo1a

The experiments outlined previously indicate that the motor and TH1 domains both play important roles in regulating Myo1a dynamics. In full-length Myo1a, these two domains are physically linked by an extended α-helix comprised of three calmodulin-binding IQ motifs, also referred to as the lever arm. Structural studies have shown that the Myo1a lever arm rotates through a large angle to amplify small conformational changes that originate in the motor domain during force generation (11,49). In addition to producing force and motion, the lever arm has also been implicated in load sensing (8,50). In this context, the lever arm plays a role in transmitting loads applied at the C-terminus to the N-terminal motor domain to promote long-lived actin binding. To determine if the lever arm plays a role in the regulation of Myo1a dynamics, we created an in-frame deletion that eliminates all three calmodulin binding sites (Δa.a.695–764, Myo1a-neckless; Fig. 1). We first expressed Myo1a-neckless in polarized LLC-PK1-CL4 epithelial cells and analyzed brush border localization using our previously reported method for the quantification of microvillar targeting, referred to as fold enrichment in microvilli (FEM) (22). Myo1a-neckless is unable to target properly to microvilli at steady state, with a FEM value of 0.85 ± 0.13 (proteins that enrich in microvilli exhibit FEM >1). We then analyzed Myo1a-neckless dynamics in live cells using SM-TIRF. Relative to full-length Myo1a, Myo1a-neckless exhibited a broad D distribution that was shifted toward higher mobility, with a peak D of 0.061 $\mu m^2/s$ and shape factor of 14.4 (Fig. 5 *A*, Table 1). Long-lived, low D events characteristic to full-length Myo1a were noticeably absent from Myo1a-neckless trajectories (Fig. 5 *A*, *inset*). Moreover, kymograph analysis of Myo1a-neckless produced traces that resembled TH1 and lacked the long-lived actin-localized events that were abundant in full-length Myo1a recordings (see Fig. 5 *C*).

The requirement for an intact lever arm suggests that mechanical coupling between the motor and TH1 domains is important for restricting the dynamics of Myo1a under normal conditions. These results also suggest the possibility that load sensing, which is mediated by the lever arm, might play a role in restricting the mobility of full-length Myo1a. To investigate how a load-sensitive motor would respond in the live cell environment probed in our SM-TIRF assays, we imaged single-molecule dynamics of 3x-mCitrine-tagged Myo1b, specifically, the splice form containing six IQ motifs, which is exquisitely sensitive to load (8,50). The observed D distribution was nearly identical to full-length Myo1a with a peak D of 0.033 $\mu m^2/s$ and a shape factor of 29 (Fig. 5 *B*, Table 1). These data suggest that in the context of our live cell single-molecule assay, Myo1a exhibits properties similar to load-sensing class 1 myosins.

DISCUSSION

These studies are the first, to our knowledge, to investigate the single-molecule dynamics of class 1 myosins in live cells. The approach described here allows direct measurement of physical parameters (e.g., D) and provides an unbiased method for determining how specific subdomains of Myo1a govern dynamics at the cell periphery. Analysis of diffusion coefficients revealed that full-length Myo1a displays limited mobility relative to TH1 and Lact-C2 (Fig. 2). The most significant difference between these constructs is the presence of the motor domain in full-length Myo1a. Mutation of motor domain residues involved in actin binding produced a rightward shift in the D distribution for Myo1a, suggesting that actin binding is restricting mobility under normal conditions (Fig. 3). This was an unexpected result for two reasons. First, previous studies had established the importance of TH1/membrane interactions in subcellular targeting, which suggested this domain alone would control single-molecule dynamics. Second, early solution kinetic measurements determined

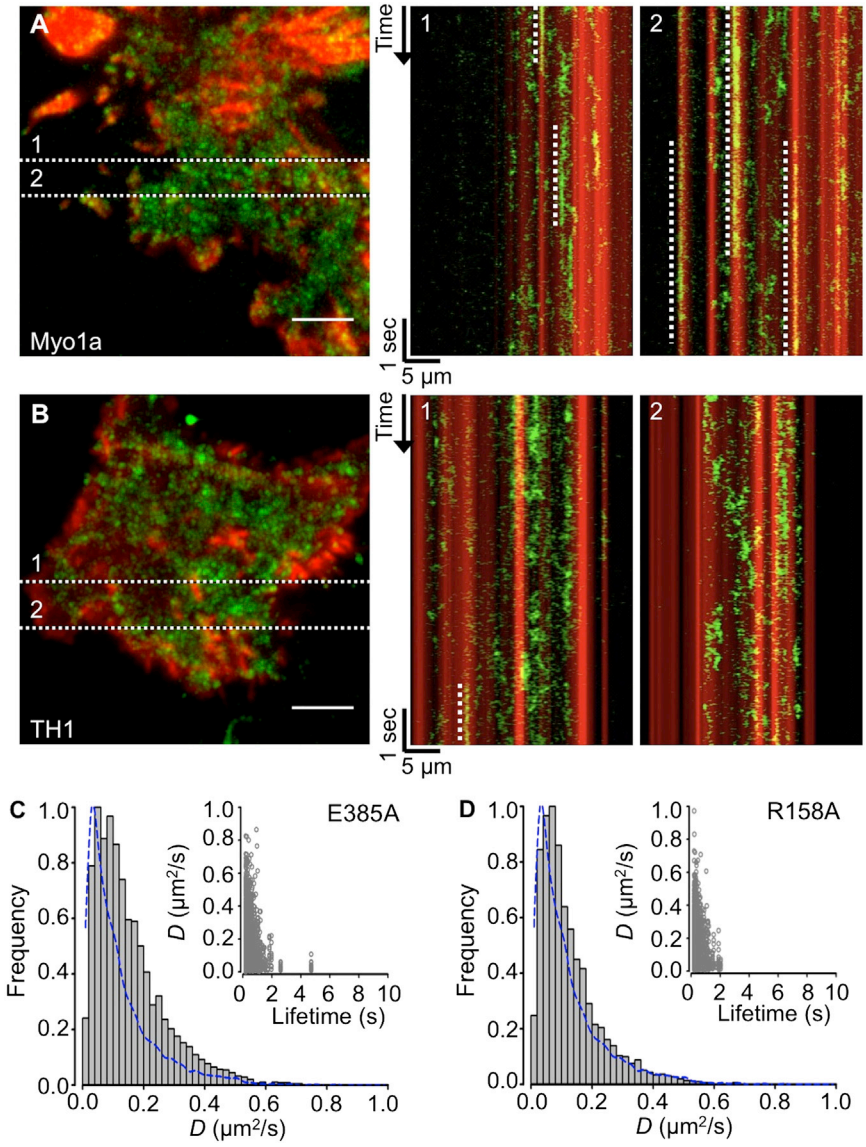

FIGURE 3 Motor domain interactions with actin reduce the mobility of full-length Myo1a. Kymographs, right, show 3x-Citrine-tagged Myo1a (*green*, *A*) or Myo1a-TH1 (*green*, *B*) merged with the mCherry-Espin (*red*) image from each corresponding cell. Cell images, left, are maximum intensity projections of image stacks. Dashed lines in projections depict location of the corresponding kymograph. Dashed lines in kymographs represent immobilized molecules. Bars are 5 μm. Histograms of *D* values for Myo1a-E385A (*C*) and Myo1a-R15A (*D*). Inset, plots of *D* versus lifetime associated with each trajectory fit to obtain *D* values. Long-lived events were lost and the numbers of near-immobile events were reduced for both mutant constructs. E385A and R158A mutations caused the overall distribution of *D* values to shift toward higher mobility. Blue dashed lines are traced outlines of Myo1a histogram density from Fig. 2 *A*.

that Myo1a purified from chicken intestinal tissue has a short actin-bound lifetime (~50 ms) and low unloaded duty ratio (<10%) (10). However, in our live cell studies, the *D* distribution for full-length Myo1a contained low mobility events lasting up to 8 s (Fig. 2 *A*) and kymography showed that Myo1a molecules colocalize on actin filaments for several seconds (Fig. 3 *A*). These data suggest that actin-bound lifetimes in live cells may be much longer than expected based on solution kinetics (10) and long enough to restrict the mobility of Myo1a. These observations might be explained by properties such as load sensing, which are known to regulate the actin-binding kinetics of closely related Myo1b (more below) (8).

These single-molecule observations also reveal a role for the lever arm in restricting the mobility of full-length Myo1a, as deletion of this domain resulted in a significant rightward shift in the *D* distribution (Fig. 5). Of importance, these experiments indicate that functional motor and TH1 domains alone are unable to recapitulate the restricted dynamics exhibited by full-length Myo1a. Thus, in the context of our single-molecule assay, the lever arm must be playing a role other than passively linking these two domains. In all myosins, the lever arm serves as a rigid extension that amplifies small conformational changes generated in the motor domain and is therefore critical for force production. For Myo1b, which is closely related to Myo1a in phylogenetic analyses (51), this structure is also important for load sensing as it allows external forces that impinge on the C-terminal TH1 domain to be communicated to the motor domain in a manner that slows detachment from actin (8). Thus, one intriguing explanation for the restricted mobility of full-length Myo1a and the effect of the lever arm deletion is that Myo1a molecules visualized in our assay may be

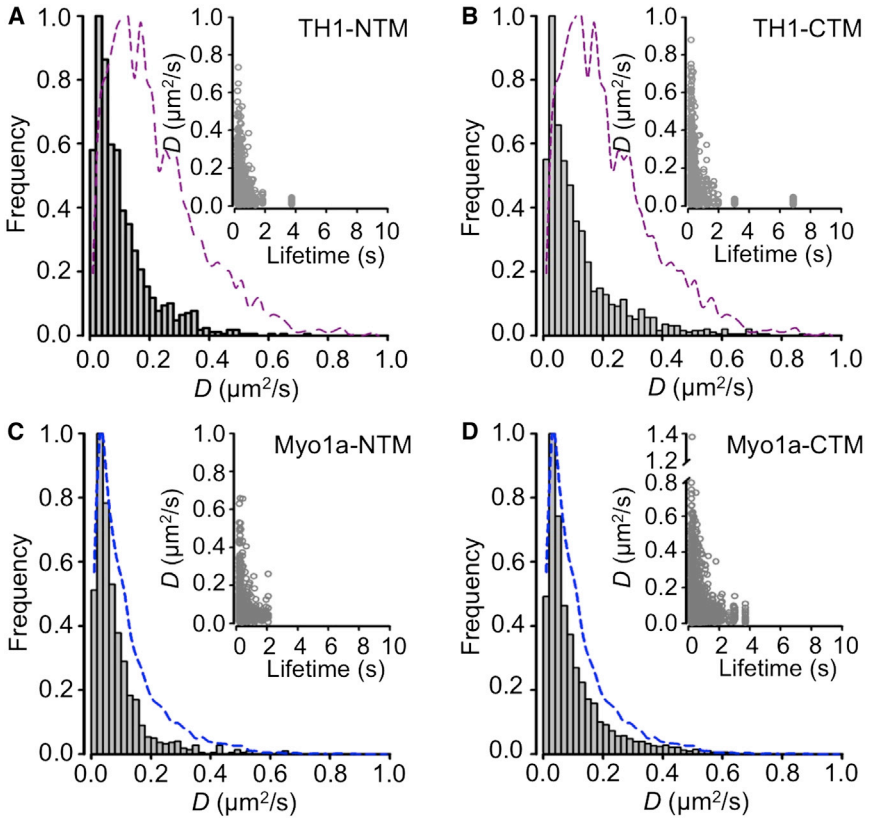

FIGURE 4 Membrane binding mutants TH1-NTM, TH1-CTM, Myo1a-NTM, and Myo1a-CTM display reduced mobility. Histograms of *D* values for TH1-NTM (*A*), TH1-CTM (*B*), Myo1a-NTM (*C*), and Myo1a-CTM (*D*). Inset, plots of *D* versus lifetime associated with each trajectory fit to obtain *D* values. Membrane binding mutations for both full-length Myo1a and TH1 resulted in loss of long-lived events and shifts toward low mobility in the overall distribution of *D* values. Purple dashed lines are traced outlines of the TH1 histogram density from Fig. 2 *B*. Blue dashed lines are traced outlines of Myo1a histogram density from Fig. 2 *A*.

under load. This, in turn, would have the effect of increasing actin-attached lifetimes, and explain the presence of unexpectedly long-lived, low mobility events in the full-length Myo1a data set. This proposal is supported by the fact that Myo1a and Myo1b show nearly identical behavior in the SM-TIRF assay (Fig. 5). Although Myo1a does exhibit biochemical and structural features that are predictive of load sensing (12), further studies are needed to unambiguously determine if Myo1a exhibits the robust tension sensing response demonstrated by Myo1b. A second possible explanation for the increased diffusional mobility of Myo1a-neckless is that the lever arm provides a binding site for a receptor at the cell cortex, perhaps a membrane protein that would facilitate the docking of Myo1a and restrict diffusion. The myristoylated calmodulin-like molecule, calmyrin, which binds to IQ motifs in the lever arm of Myo1c could be one such receptor (52). However, it is not known if such interactions are relevant for Myo1a.

Our previous studies showed that mutations to basic residues in NTM and CTM decrease the membrane-bound lifetime of TH1 in cells (22). We therefore expected these mutations to impact full-length Myo1a dynamics as well. Mutations to either motif, in the context of TH1 or full-length Myo1a constructs, significantly reduced diffusional mobility (Fig. 4). These results suggest that lifetime and mobility are uncoupled such that low mobility interactions with the membrane are possible even during brief events. These data also indicate that the multiple membrane binding sites provided by NTM and CTM promote reduced dimensionality diffusion, which keeps Myo1a close to the membrane, perhaps to facilitate the search for an appropriate binding site. Similar mechanisms have been proposed for MCAK, a kinesin motor that uses electrostatic interactions to rapidly diffuse along spindle microtubules to achieve plus end localization (53), and DNA binding proteins, which exploit diffusion to find their promoter regions and associated binding partners (54).

A recent study by Gupta et al. (55) investigated the function and dynamics of the long-tailed class 1 myosin, Myo1e, at the leading edge of spreading cells. In this work, puncta containing multiple Myo1e molecules were tracked and quantified using MSD analysis, revealing complex multimode behavior. Although the majority of Myo1e puncta demonstrated diffusive motion, examples of directed movement were also observed. The calculated velocity for directed puncta (>2 μm/s) is faster than other class 1 myosins characterized to date, and thus, it remains to be determined if this movement is driven by Myo1e motor activity. Short-tailed Myo1g analyzed in these same experiments exhibited purely diffusive behavior. These findings are generally consistent with the results we present here and support the proposal that the major mode of both short and long-tailed myosin-1 movement within the cell is diffusive in nature.

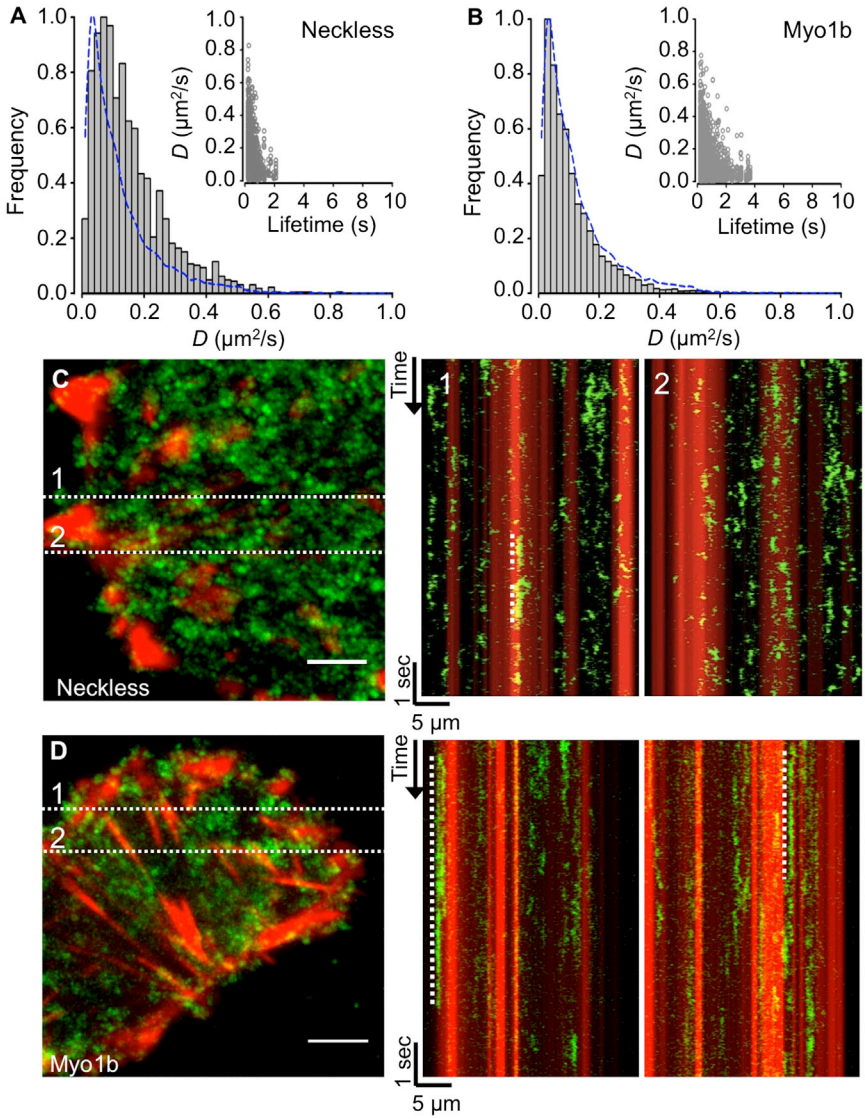

FIGURE 5 Eliminating the neck region increases the mobility of Myo1a. Histogram of *D* values for Myo1a-Neckless (*A*) or full-length Myo1b (*B*). Inset, plot of *D* versus lifetime associated with each trajectory fit to obtain *D* values. Blue dashed lines are traced outlines of Myo1a histogram density from Fig. 2 *A*. Kymograph analysis of Myo1a-Neckless (*C*) or Myo1b (*D*). Kymographs, right, show 3x-Citrine-tagged construct (*green*) merged with the mCherry-Espin (*red*) image from each corresponding cell. Cell images, left, are maximum projections of image stacks. Dashed horizontal lines represent location of the corresponding kymograph. In kymographs, dashed vertical lines depict low mobility events. Bars are 5 μm.

Taken together, the data presented here suggest that the motor and TH1 domains function antagonistically to control Myo1a dynamics in live cells (Fig. 6). That is, motor domain interactions with F-actin restrict diffusional mobility, whereas TH1 domain interactions with the membrane promote mobility. We also show that the lever arm plays a role in coordinating this antagonism, but not merely as a passive linker of these two domains. Because lever arm deletion phenocopies the impact of actin-binding mutations in the motor domain, our data suggest that the lever arm functions with the motor domain to restrict mobility. Based on the similarities between Myo1a and Myo1b in the SM-TIRFM assay, it is tempting to speculate that the Myo1a lever arm can mediate load sensing in live cells. However, single-molecule studies using a load clamp optical trap are needed to determine if Myo1a shares the load-sensing properties of Myo1b or Myo1c. Future studies will also focus on applying the single-molecule imaging approach described here in the context of parallel actin bundle supported protrusions such as microvilli, the physiological site of function for Myo1a.

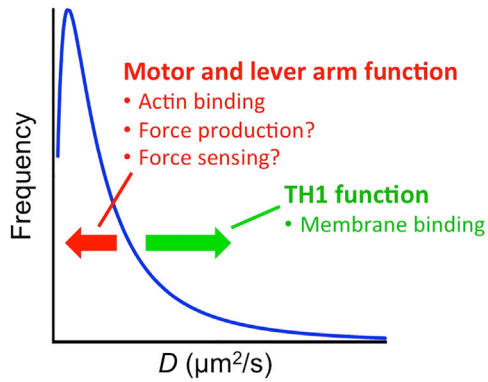

FIGURE 6 Summary of factors controlling the dynamics of myosin-1.

SUPPORTING MATERIAL

One figure is available at http://www.biophysj.org/biophysj/supplemental/S0006-3495(14)00012-5.

The authors thank all members of the Tyska laboratory for advice and support. SM-TIRF microscopy was performed in part through the use of the VUMC Epithelial Biology Center Imaging Resource.

This work was supported by American Heart Association (AHA) predoctoral fellowship (J.N.M.), AHA grant-in-aid 12GRNT12050314 (M.J.T.), the VUMC Digestive Diseases Research Center DK058404, a Vanderbilt University IDEAS award (M.J.T.), and National Institutes of Health DK075555 and DK095811 (M.J.T.). This work was also supported by NSF/DMS 0970008 from the National Science Foundation (A.K.K.) and utilized the core(s) of the Vanderbilt Diabetes Research and Training Center funded by grant DK020593 from the National Institute of Diabetes and Digestive and Kidney Disease. The funding sources had no role in the study design, collection, analysis or interpretation of data, writing the report, or the decision to submit the paper for publication.

REFERENCES

1. Nambiar, R., R. E. McConnell, and M. J. Tyska. 2009. Control of cell membrane tension by myosin-I. *Proc. Natl. Acad. Sci. USA.* 106:11972–11977.
2. Gillespie, P. G., and J. L. Cyr. 2004. Myosin-1c, the hair cell's adaptation motor. *Annu. Rev. Physiol.* 66:521–545.
3. Almeida, C. G., A. Yamada, …, E. Coudrier. 2011. Myosin 1b promotes the formation of post-Golgi carriers by regulating actin assembly and membrane remodelling at the trans-Golgi network. *Nat. Cell Biol.* 13:779–789.
4. Bose, A., A. Guilherme, …, M. P. Czech. 2002. Glucose transporter recycling in response to insulin is facilitated by myosin Myo1c. *Nature.* 420:821–824.
5. Greenberg, M. J., and E. M. Ostap. 2013. Regulation and control of myosin-I by the motor and light chain-binding domains. *Trends Cell Biol.* 23:81–89.
6. McConnell, R. E., and M. J. Tyska. 2010. Leveraging the membrane - cytoskeleton interface with myosin-1. *Trends Cell Biol.* 20:418–426.
7. De La Cruz, E. M., and E. M. Ostap. 2009. Kinetic and equilibrium analysis of the myosin ATPase. *Methods Enzymol.* 455:157–192.
8. Laakso, J. M., J. H. Lewis, …, E. M. Ostap. 2008. Myosin I can act as a molecular force sensor. *Science.* 321:133–136.
9. Greenberg, M. J., T. Lin, …, E. M. Ostap. 2012. Myosin IC generates power over a range of loads via a new tension-sensing mechanism. *Proc. Natl. Acad. Sci. USA.* 109:E2433–E2440.
10. Jontes, J. D., R. A. Milligan, …, E. M. Ostap. 1997. Kinetic characterization of brush border myosin-I ATPase. *Proc. Natl. Acad. Sci. USA.* 94:14332–14337.
11. Jontes, J. D., E. M. Wilson-Kubalek, and R. A. Milligan. 1995. A 32 degree tail swing in brush border myosin I on ADP release. *Nature.* 378:751–753.
12. Veigel, C., L. M. Coluccio, …, J. E. Molloy. 1999. The motor protein myosin-I produces its working stroke in two steps. *Nature.* 398: 530–533.
13. Tang, N., T. Lin, and E. M. Ostap. 2002. Dynamics of myo1c (myosin-ibeta) lipid binding and dissociation. *J. Biol. Chem.* 277:42763–42768.
14. McKenna, J. M., and E. M. Ostap. 2009. Kinetics of the interaction of myo1c with phosphoinositides. *J. Biol. Chem.* 284:28650–28659.
15. Tyska, M. J., and M. S. Mooseker. 2002. MYO1A (brush border myosin I) dynamics in the brush border of LLC-PK1-CL4 cells. *Biophys. J.* 82:1869–1883.
16. Benesh, A. E., R. Nambiar, …, M. J. Tyska. 2010. Differential localization and dynamics of class I myosins in the enterocyte microvillus. *Mol. Biol. Cell.* 21:970–978.
17. Tang, N., and E. M. Ostap. 2001. Motor domain-dependent localization of myo1b (myr-1). *Curr. Biol.* 11:1131–1135.
18. Patino-Lopez, G., L. Aravind, …, S. Shaw. 2010. Myosin 1G is an abundant class I myosin in lymphocytes whose localization at the plasma membrane depends on its ancient divergent pleckstrin homology (PH) domain (Myo1PH). *J. Biol. Chem.* 285:8675–8686.
19. Hokanson, D. E., J. M. Laakso, …, E. M. Ostap. 2006. Myo1c binds phosphoinositides through a putative pleckstrin homology domain. *Mol. Biol. Cell.* 17:4856–4865.
20. Hokanson, D. E., and E. M. Ostap. 2006. Myo1c binds tightly and specifically to phosphatidylinositol 4,5-bisphosphate and inositol 1,4,5-trisphosphate. *Proc. Natl. Acad. Sci. USA.* 103:3118–3123.
21. Komaba, S., and L. M. Coluccio. 2010. Localization of myosin 1b to actin protrusions requires phosphoinositide binding. *J. Biol. Chem.* 285:27686–27693.
22. Mazerik, J. N., and M. J. Tyska. 2012. Myosin-1A targets to microvilli using multiple membrane binding motifs in the tail homology 1 (TH1) domain. *J. Biol. Chem.* 287:13104–13115.
23. Brzeska, H., K. J. Hwang, and E. D. Korn. 2008. Acanthamoeba myosin IC colocalizes with phosphatidylinositol 4,5-bisphosphate at the plasma membrane due to the high concentration of negative charge. *J. Biol. Chem.* 283:32014–32023.
24. Feeser, E. A., C. M. Ignacio, …, E. M. Ostap. 2010. Myo1e binds anionic phospholipids with high affinity. *Biochemistry.* 49:9353–9360.
25. Mazzolini, R., H. Dopeso, …, D. Arango. 2012. Brush border myosin Ia has tumor suppressor activity in the intestine. *Proc. Natl. Acad. Sci. USA.* 109:1530–1535.
26. Cai, D., K. J. Verhey, and E. Meyhöfer. 2007. Tracking single Kinesin molecules in the cytoplasm of mammalian cells. *Biophys. J.* 92:4137–4144.
27. Vallotton, P., A. Ponti, …, G. Danuser. 2003. Recovery, visualization, and analysis of actin and tubulin polymer flow in live cells: a fluorescent speckle microscopy study. *Biophys. J.* 85:1289–1306.
28. Saxton, M. J. 1997. Single-particle tracking: the distribution of diffusion coefficients. *Biophys. J.* 72:1744–1753.
29. Wade, W. F., J. H. Freed, and M. Edidin. 1989. Translational diffusion of class II major histocompatibility complex molecules is constrained by their cytoplasmic domains. *J. Cell Biol.* 109:3325–3331.
30. Mooseker, M. S. 1985. Organization, chemistry, and assembly of the cytoskeletal apparatus of the intestinal brush border. *Annu. Rev. Cell Biol.* 1:209–241.
31. Tyska, M. J., A. T. Mackey, …, M. S. Mooseker. 2005. Myosin-1a is critical for normal brush border structure and composition. *Mol. Biol. Cell.* 16:2443–2457.
32. McConnell, R. E., and M. J. Tyska. 2007. Myosin-1a powers the sliding of apical membrane along microvillar actin bundles. *J. Cell Biol.* 177:671–681.
33. Tyska, M. J., and M. S. Mooseker. 2004. A role for myosin-1A in the localization of a brush border disaccharidase. *J. Cell Biol.* 165:395–405.
34. Kravtsov, D. V., C. Caputo, …, N. A. Ameen. 2012. Myosin Ia is required for CFTR brush border membrane trafficking and ion transport in the mouse small intestine. *Traffic.* 13:1072–1082.
35. Yeung, T., G. E. Gilbert, …, S. Grinstein. 2008. Membrane phosphatidylserine regulates surface charge and protein localization. *Science.* 319:210–213.
36. Kenworthy, A. K., B. J. Nichols, …, J. Lippincott-Schwartz. 2004. Dynamics of putative raft-associated proteins at the cell surface. *J. Cell Biol.* 165:735–746.
37. Jacobson, K., A. Ishihara, and R. Inman. 1987. Lateral diffusion of proteins in membranes. *Annu. Rev. Physiol.* 49:163–175.

38. Veliz, L. A., C. A. Toro, …, S. Brauchi. 2010. Near-membrane dynamics and capture of TRPM8 channels within transient confinement domains. *PLoS ONE.* 5:e13290.

39. Bürli, T., K. Baer, …, J. M. Fritschy. 2010. Single particle tracking of alpha7 nicotinic AChR in hippocampal neurons reveals regulated confinement at glutamatergic and GABAergic perisynaptic sites. *PLoS ONE.* 5:e11507.

40. Haggie, P. M., J. K. Kim, …, A. S. Verkman. 2006. Tracking of quantum dot-labeled CFTR shows near immobilization by C-terminal PDZ interactions. *Mol. Biol. Cell.* 17:4937–4945.

41. Howard, J. 2001. Mechanics of Motor Proteins and the Cytoskeleton. Sinauer Associates, New York.

42. Foth, B. J., M. C. Goedecke, and D. Soldati. 2006. New insights into myosin evolution and classification. *Proc. Natl. Acad. Sci. USA.* 103:3681–3686.

43. Smith, C. A., and I. Rayment. 1996. X-ray structure of the magnesium(II).ADP.vanadate complex of the *Dictyostelium discoideum* myosin motor domain to 1.9 A resolution. *Biochemistry.* 35:5404–5417.

44. Shimada, T., N. Sasaki, …, K. Sutoh. 1997. Alanine scanning mutagenesis of the switch I region in the ATPase site of *Dictyostelium discoideum* myosin II. *Biochemistry.* 36:14037–14043.

45. Sasaki, N., T. Shimada, and K. Sutoh. 1998. Mutational analysis of the switch II loop of *Dictyostelium* myosin II. *J. Biol. Chem.* 273:20334–20340.

46. Weil, D., S. Blanchard, …, C. Petit. 1995. Defective myosin VIIA gene responsible for Usher syndrome type 1B. *Nature.* 374:60–61.

47. Aschenbrenner, L., S. N. Naccache, and T. Hasson. 2004. Uncoated endocytic vesicles require the unconventional myosin, Myo6, for rapid transport through actin barriers. *Mol. Biol. Cell.* 15:2253–2263.

48. Belyantseva, I. A., E. T. Boger, …, T. B. Friedman. 2005. Myosin-XVa is required for tip localization of whirlin and differential elongation of hair-cell stereocilia. *Nat. Cell Biol.* 7:148–156.

49. Jontes, J. D., and R. A. Milligan. 1997. Brush border myosin-I structure and ADP-dependent conformational changes revealed by cryoelectron microscopy and image analysis. *J. Cell Biol.* 139:683–693.

50. Laakso, J. M., J. H. Lewis, …, E. M. Ostap. 2010. Control of myosin-I force sensing by alternative splicing. *Proc. Natl. Acad. Sci. USA.* 107:698–702.

51. Berg, J. S., B. C. Powell, and R. E. Cheney. 2001. A millennial myosin census. *Mol. Biol. Cell.* 12:780–794.

52. Tang, N., T. Lin, …, E. M. Ostap. 2007. CIB1 and CaBP1 bind to the myo1c regulatory domain. *J. Muscle Res. Cell Motil.* 28:285–291.

53. Helenius, J., G. Brouhard, …, J. Howard. 2006. The depolymerizing kinesin MCAK uses lattice diffusion to rapidly target microtubule ends. *Nature.* 441:115–119.

54. Gorman, J., and E. C. Greene. 2008. Visualizing one-dimensional diffusion of proteins along DNA. *Nat. Struct. Mol. Biol.* 15:768–774.

55. Gupta, P., N. C. Gauthier, …, M. Sheetz. 2013. Myosin 1E localizes to actin polymerization sites in lamellipodia, affecting actin dynamics and adhesion formation. *Biol. Open.* 2:1288–1299.